Silica Nanobubbles Containing an Organic Dye in a Multilayered Organic/Inorganic Heterostructure with Enhanced Luminescence

M. Lal, L. Levy, K. S. Kim, G. S. He, X. Wang, Y. H. Min, S. Pakatchi, and P. N. Prasad*

Photonics Research Laboratory, Departments of Chemistry and Physics, State University of New York at Buffalo, Buffalo, New York 14260

Received February 28, 2000. Revised Manuscript Received July 14, 2000

We report the preparation, luminescent properties, and bioimaging applications of a novel zinc sulfide (core)-two-photon dye−silica (shell) multilayered heterostructure. The method utilizes reverse micelles synthesis involving multistep reactions as a result of which composite nanoparticles having different sizes and morphology can be obtained. The size of these composite nanoparticles is typically 15−30 nm. An increase in the luminescence intensity (∼70 times higher) and in fluorescence lifetime is observed for the dye encapsulated within the silica nanobubble. Photobleaching results indicate that the dye is truly encapsulated and the silica shell provides a barrier to penetration of oxygen, thereby making the dye more photostable. The application of these particles as nanoprobes for bioimaging of cells using two-photon laser scanning microscopy is also presented.

Introduction

The use of inorganic nanoparticles (metals and semiconductors) as nanoprobes[1] is a newly emerging field that has already exhibited its potential in applications as[2,3] sensors and biosensors and in cell imaging, DNA sequencing, immunoassay, or other types of analyses.[4] There is also widespread interest in incorporation of dyes within inorganic matrixes, mainly for applications as solid-state laser devices, nonlinear optical materials, and optical memory devices.[5] Another interesting new development has been the incorporation of dyes or fluorescent labels within nanoparticles[6] for optical probe applications involving detection of biomolecules and biomolecular processes. Recently, two-photon processes[7−16] have drawn considerable interest for a wide range of applications such as in optical data storage,[7−10] two-photon laser scanning microscopy,[11−15] and three-dimensional microfabrication.[16] The use of two-photon excitation microscopy[11−15] has advantages over the conventional single-photon laser scanning microscopy in minimizing photobleaching and photodamage, which are the ultimate limiting factors in imaging living cells. However, most two-photon dyes are not water dispersable or the quantum yield of their fluorescence is considerably reduced in water.

We describe here a novel approach to prepare silica nanobubbles containing a two-photon dye that encapsulates the core of a zinc sulfide particle through a thiol group. We characterize the fluorescence properties of such particles and demonstrate their application in bioimaging. Because most two-photon dyes are highly hydrophobic, encapsulation of these dyes within silica increases their dispersability in water. Also, by providing an inert barrier to the influence of an external environment, encapsulation of the dye within silica leads to an enhancement in emission by minimizing the solvent effects responsible for nonradiative decay mechanisms.

In our work, the synthesis of such a dye-doped composite nanoparticle is acheived by carrying out reaction within a reverse micellar cavity. This approach of nanocompartmentalization[17] has already been used extensively in the area of material science for preparing various metallic nanoparticles,[18−20] semiconductor nano-

(1) Bruchez, M.; Moronne, M.; Gin, P.; Weiss, S.; Alivisatos, A. P. *Science* **1998**, *281*, 2013−2015.
(2) Miltenyi, S.; Muller, W.; Weichel, W.; Radbruch, A. *Cytometry* **1990**, *11*, 231.
(3) Alivisatos, A. P. et al. *Nature* **1996**, *382*, 609.
(4) Nie, S.; Chan, C. W. C. *Science* **1998**, *281*, 2016−2018.
(5) Reisfield, R.; Yariv, E.; Minti, H. *Opt. Mater.* **1997**, *8*, 31.
(6) (a)Clark, H. A.; Barker, S. L. R.; Brasuel, M.; Miller, M. T.; Monson, E.; Parus, S.; Shi, Z. Y.; Song, A.; Thorsrud, B.; Kopelman, R.; Ade, A.; Meixner, W.; Athey, B.; Hoyer, M.; Hill, D.; Lightle, R.; Philbert, M. A. *Sens. Actuators B* **1998**, *51*, 12−16. (b)Makarova, O. V.; Ostafin, A. E.; Miyoshi, H.; Norris, J. R.; Meisel, D. *J. Phys. Chem. B* **1999**, A.-E.
(7) Parthenopoulos, D. A.; Rentzepis, P. M. *Science* **1989**, *245*, 843−845.
(8) Parthenopoulos, D. A.; Rentzepis, P. M. *J. Appl. Phys.* **1990**, *68*, 5814−5818.
(9) Dvornikov, A. S.; Rentzepis, P. M. *Opt. Commun.* **1995**, *119*, 341−346.
(10) Joshi, M. P.; Pudavar, H. E.; Swiatkiewicz, J.; Prasad, P. N.; Reinhardt, B. A. *Appl. Phys. Lett.* **1999**, *74*, 170.
(11) Bhawalkar, J. D.; He, G. S.; Prasad, P. N. *Rep. Prog. Phys.* **1996**, *59*, 1041.
(12) Denk, W.; Strickler, J. H.; Webb, W. W. *Science* **1990**, *248*, 73.
(13) Yuste, R.; Denk, W. *Nature* **1995**, *375*, 682−684.
(14) Piston, D. W. *Trends Cell Biol.* **1999**, *9*, 66−69.
(15) Williams, R.; Piston, D.; Webb, W. W. *FASEB* **1994**, *8*, 804−813
(16) Pudavar, H. E.; Joshi, M. P.; Prasad, P. N.; Reinhardt, B. A. *Appl. Phys. Lett.* **1999**, *74*, 1338.
(17) Towey, T. F.; Khan-Lodhi, A. N.; Robinson, B. H.; *J. Chem. Soc.* **1990**, *86*, 3757.
(18) Taleb, A.; Petit, C.; Pileni, M. P. *Chem. Mater.* **1997**, *9*, 950−959.

10.1021/cm000178k CCC: $19.00
Published on Web 08/19/2000

clusters,[21−23] and polymeric nanoparticles.[24−26] The interest stems mainly from the diversity in the organized structures that are formed under different compositional and operational conditions[27,28] using the reverse micelles approach. Reduction of the particle size to a nanometer level has potential benefits, which manifests by remarkably changing the physicochemical properties, the most noticeable being the quantum size effect[29] observed in semiconductor nanoparticles. The other effects are enhanced electric and magnetic properties of metallic particles and nanoclusters.[30] The highlighting feature of reverse micelles synthesis is size tunability, which arises as a result of confining a reaction to nanometer-sized aqueous droplets characterized by a size parameter, W_0 ($W_0 = [H_2O]/[\text{Surfactant}]$). The exchange rate and dynamics of these droplets influence the particle growth and nucleation, thereby governing the particle size.[31] The changes in particle size can also be obtained by modifying the absolute and relative reactant concentrations, which is expected to be of significance in the formation of complex structures and composites.[32,33]

Using reverse micelles mediated synthesis, we have prepared ZnS/dye/SiO_2 heterostructured nanoparticles through a multistep reaction. Specifically, by subsequent reaction and chemical processing within the cavity, we made inorganic−organic particles containing a zinc sulfide core attached to a two-photon dye ASPI−SH (1-Methyl-4-(E)-2-{4-[methyl(2-sulfanylethyl)amino]-phenyl}ethenyl)pyridinium iodide), which is attached to the semiconductor through the thiol group. ASPI−SH belongs to a general family of hemicyanine dyes (containing short alkyl chains such as amino styryl pyridine derivatives) and exhibiting a very high two-photon absorption cross section more than 2 orders of magnitude higher than those of previously reported compounds.[34,35] The most attractive feature of this dye is its utility as a biological probe because it shows two-photon-induced emission with an IR (infrared) source. As a result, there is practically no absorption from the background (biological fluid). Zinc sulfide was chosen as the semiconductor because its band gap is well separated from that of the chromophore. In other words, there is no spectral overlap between zinc sulfide and the dye. During the reaction, the nucleus of zinc sulfide grows to a desired/required size (W_0), and then the surface of these nanocrystallites is passivated or capped through covalent addition of the dye (ASPI−SH) thiol where the thiol group acts as a growth moderator.[36] This property stems from the ability of thiolate ions to bind to the metal ions on the semiconductor surface, thereby effectively inhibiting the growth of the semiconductor nanoparticles.[36,37] This process was followed by the introduction of a sol−gel silica precursor, tetraethoxy orthosilicate (TEOS), which undergoes hydrolysis in the aqueous core forming a silica shell around the dye-capped zinc sulfide particles. The advantage of using TEOS as the silica precursor is its relatively slow and controllable rate of reaction. Furthermore, the reverse micelles technique is versatile and can be used for the synthesis of other kinds of hybrid materials.

There are several advantages of using silica shells as stabilizers. Unlike polymers, it is not subject to microbial attack and there is no swelling or porosity change occurring in these particles with the change of pH.[38] Silica is chemically inert and, therefore, does not affect the redox reaction at the core surface. The shell is optically transparent; furthermore, the shell prevents coagulation during chemical reactions and concentrated dispersions of nanosized semiconductors can be made. Also, the silica shell acts as a stabilizer, limiting the effect of the outside environment on the core particles. This is particularly important for two-photon dyes, which are sensitive to certain solvents, especially water, that quenches the emission due to certain nonradiative decay processes. Most important, however is the ease of synthesis as no special conditions (e.g., initiator, temperature) are required for the synthesis.

Photobleaching[39] and thermally induced degradation[40] are the problems commonly encountered in laser dyes that reduce the operational lifetime of the dye. By encapsulation of a dye within the silica shell, where silica is chemically and thermally inert, photobleaching and photodegradation of the dye can also be minimized. This advantage has been demonstrated in our work. Another advantage of using silica is the introduction of a specific surface functionality,[41−43]which can be obtained by modifying the surface hydroxyls on the silica surface with amines, thiols, carboxyls, and methacrylate. This modification can facilitate the incorporation of these particles into nonpolar solvents, glasses, and polymeric matrixes.

(19) Petit, C.; Lixon, P.; Pileni, M. P. *J. Phys. Chem.* **1993**, *97*, 12974.
(20) Lisiecki, I.; Pileni, M. P. *J. Phys. Chem.* **1995**, *99*, 5077.
(21) Levy, L.; Hochepied, J. F.; Pileni, M. P. *J. Phys. Chem.* **1996**, *100*, 18322−18326.
(22) Hirai, T.; Sato, H.; Komasawa, I. *Ind. Eng. Chem. Res.* **1994**, *33*, 3262.
(23) Meyer, M.; Walberg, C.; Kurihara, K.; Fendler, J. H. *J. Chem. Soc., Chem. Commun.* **1984**, *18*, 2641.
(24) Stoffer, J. C.; Bone, T. J. *Polym. Sci. Polym. Ed.* **1980**, *18*, 2641.
(25) Lal, M.; Kumar, N. D.; Joshi, M. P.; Prasad, P. N. *Chem. Mater.* **1998**, *10*, 1065.
(26) Leong, Y. S.; Candau, F. *J. Phys. Chem.* **1982**, *86*, 2269.
(27) Rees, G. D.; Gowing, R. E.; Hammond, S. J.; Robinson, B. H. *Langmuir* **1999**, *15*, 1993−2002.
(28) Luisi, P. L.; Scartazzini, R.; Pileni, M. P.; Robinson, B. H. *Biochim. Biophys. Acta* **1988**, *947*, 209.
(29) Rosetti, R.; Hull, R.; Gibson, J. M.; Brus, L. E. *J. Chem. Phys.* **1985**, *82*, 552.
(30) Lopez-Quintela, M. A.; Rivas, J. *Curr. Opin. Colloid Interface Sci.* **1996**, *1*, 806.
(31) Eastoe, J.; Warne, B. *Curr. Opin. Colloid Interface Sci.* **1996**, *1*, 800.
(32) Qi, L.; Ma, J.; Cheng, H.; Zhao, Z. *Colloids Surf.* **1996**, *108*, 117.
(33) Chang, S.; Liu, L.; Asher, S. A. *J. Am. Chem. Soc.* **1993**, *116*, 6739.
(34) Zhao, C. F.; Gvishi, R.; Narang, U.; Ruland, G.; Prasad, P. N. *J. Phys. Chem.* **1996**, *100*, 4526.
(35) Narang, U.; Zhao, C. F.; Bhawalkar, J. D.; Bright, F. V.; Prasad, P. N. *J. Phys. Chem.* **1996**, *100*, 4521.
(36) Swayambunathan, V.; Hayes, D.; Schmidt, K. H.; Liao, Y. X.; Miesel, D. *J. Am. Chem. Soc.* **1990**, *112*, 3831−3837.
(37) Fischer, C. H.; Henglein, A. *J. Phys. Chem.* **1989**, *93*, 5578−5581.
(38) Jain, T. K.; Roy, I.; De, T. K.; Maitra, A. N. *J. Am. Chem. Soc.* **1998**, *120*, 11092.
(39) Kim, H. K.; Kang, S. J.; Choi, S. K.; Min, Y. H.; Yoon, C. S. *Chem. Mater.* **1999**, *11*, 779−788.
(40) Garcia, J.; Ramirez, E.; Mondragon, M. A.; Ortega, R.; Loza, P.; Campero, A. *J. Sol−Gel Sci. Technol.* **1998**, *13*, 657−661.
(41) Badley, R. D.; Warren, T. F.; McEnroe, F. J.; Assink, R. A. *Langmuir* **1990**, *6*, 792−801.
(42) Blaaderen, A. V.; Vrij, A. *J. Colloid Interface Sci.* **1993**, *156*, 1−18.
(43) Markowitz, M. A.; Schoen, P. E.; Kust, P.; Gaber, B. P. *Colloids Surf.* **1999**, *150*, 85−94.

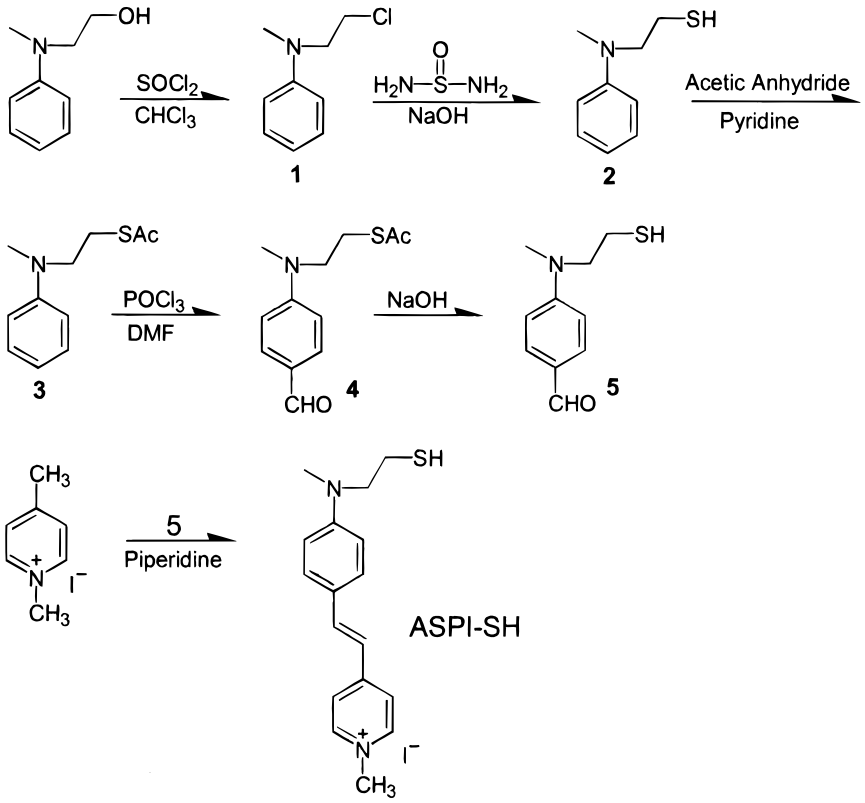

Figure 1. Schematic representation of the synthesis of two-photon dye ASPI−SH (1-methyl-4-(E)-2-{4-[methyl(2-sulfanylethyl)-amino]phenyl}-1-ethenyl)pyridinium iodide).

Experimental Section

Materials. Sodium bis(2-ethylhexyl) sulfosuccinate (AOT), 2,2,4-trimethylpentane (isooctane), zinc nitrate, sodium sulfide nonahydrate, tetraethoxysilane (TEOS), ammonium hydroxide, and dimethyl formamide were all obtained from Aldrich at the highest purity available and used without purification. The two-photon dye ASPI−SH was synthesized in our laboratory. The synthesis and the schematic representation of the route are given in Figure 1.

Synthesis of Two-Photon Dye, ASPI−SH. All starting materials were purchased from Aldrich Chemicals, except 2-(*N*-methylanilino)ethanol (Pfaltz & Bauer Chemicals). Pyridine, piperidine, and thionyl chloride were used after distillation. Other chemicals were used without purification.

***N*-(2-Chloroethyl)-*N*-methyl-*N*-phenylamine (2).** To a solution of 10 g (66 mmol) of 2-(*N*-methylanilino)ethanol in 50 mL of chloroform was added 8.7 g (73 mmol) of thionyl chloride at room temperature. After the addition of thionyl chloride was complete, the mixture was stirred for another hour at 70 °C followed by cooling and concentrating the reaction mixture in a vacuum to give a dark oily product. The dark oily crude product was dissolved in 300 mL of ethyl acetate and extracted with water. The organic layer was washed several times with water and sodium acetate and dried over anhydrous magnesium sulfate. Analytically pure compound **1** was obtained after passing through a silica gel followed by removing the solvent, at a yield of 89%. ^{1}H NMR ($CDCl_3$): δ 7.26 (t, 2H), 6.72 (t, 2H), 6.6 (d, H), 3.68−3.61 (m, 4H), 3.01 (s, 3H) ppm. Anal. Calcd. For $C_9H_{12}ClN$: C, 63.72; H, 7.13; N, 8.26. Found: C, 63.72; H, 7.16; N, 8.20.

2-(Methylanilino)-1-ethanethiol. To 10 g (60 mmol) of compound 1, a solution of 4.56 g (60 mmol) of thiourea in 60 mL of ethanol was added. The reaction mixture was heated to reflux overnight and later cooled to room temperature. A solution of 2.5 g of sodium hydroxide in 5 mL of water was added dropwise until the pH of the solution reached 7 and the dark color of the reaction mixture became pale brown. A heavy brown oil separated, was dissolved in ethyl ether, and then was extracted from water. The combined ether layer was washed with water and sodium acetate and dried over anhydrous sodium sulfate. After the solvent was removed, compound **2** was obtained as a clear brown viscous oil with a yield of 54%. ^{1}H NMR ($CDCl_3$): δ 7.25 (t, 2H), 6.71 (t, 2H), 6.60 (d, H), 3.51 (t, 2H), 2. 95 (s, 3H), 2. 72 (t, 2H), 1.36 (t, 1H). Anal. Calcd. For $C_9H_{13}NS$: C, 64.62; H, 7.83; N, 8.37. Found: C, 64.91; H, 7.85; N, 8.40.

2-(Methylanilino)ethyl Ethanethioate. A solution consisting of 15 g (89.7 mol) of compound **2**, 18.3 g (180 mmol) of acetic anhydride, and 14.2 g (180 mmol) of pyridine was stirred and refluxed for 4 h. The solution was then poured into ice cold water, and the resulting mixture was extracted with ethyl acetate. The organic portion was washed with water and brine, then with a 5% HCl solution, and again with water. Removing the combined organic layer after drying over anhydrous magnesium sulfate gave a pale brown oil product, **3**, with a yield of 83%. ^{1}H NMR ($CDCl_3$): δ 7.25 (t, 2H), 6.79−6.70 (m, 3H), 3.54 (t, 2H), 3.10 (s, 3H), 3.0 (t, 2H), 2.37 (s, 3H). Anal. Calcd. For $C_{11}H_{15}NOS$: C, 63.12; H, 7.22; N, 6.69. Found: C, 63.03; H, 7.19; N, 7.01.

2-[4-Formyl(methyl)anilino]ethyl Ethanethioate. To a solution of 70 mL of dimethylformamide in a dry ice bath was added 7.3 g (47.6 mmol) of phosphorus oxychloride dropwise under a nitrogen atmosphere. The solution was brought up to room temperature and stirred for 30 min. Into this solution 9 g (43 mmol) of compound **3** was added and stirred at a temperature of 90 °C for 2 h. After the temperature was cooled down to 0 °C, the reaction mixture was carefully poured into ice-cold water. The resulting mixture was extracted with ethyl ether, washed with sodium acetate solution and water, and dried over anhydrous sodium sulfate. After the solvent was removed under reduced pressure, compound **4** was obtained as a yellow viscous oil with a yield of 61%. ^{1}H NMR ($CDCl_3$): δ 9.75 (s, 1H), 7.77 (d, 2H), 6.81 (d, 2H), 3.56 (t, 2H), 3.10 (s, 3H), 3.01 (t, 2H), 2.37 (s, 3H). Anal. Calcd. For $C_{12}H_{15}NO_2S$: C, 60.73; H, 6.37; N, 5.90. Found: C, 60.59; H, 6.38; N, 5.98.

4-[Methyl(2-sulfanylethyl)anilino]benzaldehyde. Compound **4** (7 g, 29.5 mmol) was dissolved in 60 mL of 95% ethanol. To this, a solution of 1.2 g (29.5 mmol) of sodium

hydroxide in 3 mL of water was added and the resulting mixture was heated and refluxed for 1 h. The solution was concentrated and the remaining syrup was extracted with ethyl ether. The combined extracts were dried over anhydrous magnesium sulfate, resulting in a pale brown viscous oil, compound **5**, with a yield of 78%. ^{1}H NMR ($CDCl_3$): δ 9.75 (s, 1H), 7.76 (d, 2H), 6.73 (d, 2H), 3.62 (t, 2H), 3.10 (s, 3H), 2.76 (t, 2H), 1.59 (t, 1H). Anal. Calcd. For $C_{10}H_{13}NOS$: C, 61.50; H, 6.71; N, 7.17. Found: C, 61.34; H, 6.65; N, 7.09.

ASPI−SH. Into a solution consisting of 5 g (25.6 mmol) of compound **5** and 6.1 g (25.6 mmol) of 1,4-dimethyl pyridinium iodide in 70 mL of absolute ethanol was added 5 drops of piperidine as a catalyst. The resulting reaction mixture was heated to reflux overnight. After cooling, the mixture was filtered to collect the solid followed by washing with ethanol. The crude product was recrystallized twice from ethanol to give red crystals of ASPI−SH.

NMR ^{1}H NMR ($CDCl_3$): δ 8.71 (d, 2H), 7.02 (d, 1H), 7.68 (d, 1H), 6.75 (d, 2H), 6.62 (d, 2H), 6. 42 (d, 2H), 4.10 (s, 3H), 3.61 (t, 2H), 2.98 (s, 3H), 2.76 (t, 2H), 1.58 (s, 1H). Anal. Calcd. For $C_{17}H_{21}IN_2S$: C, 71.54; H, 7.42; N, 9.81. Found: C, 71.39, H, 7.30; N, 9.9. mp 251 °C decomposition.

Synthesis of Multistep Dye-Encapsulated Zinc Sulfide−Silica Nanocomposites. The first step in the synthesis of such nanocomposites was the formation of zinc bis(2-ethylhexyl)sulfosuccinate, also referred to as $Zn(AOT)_2$ produced by direct ion substitution of sodium bis(2-ethylhexylsulfosuccinate) or Na-AOT.[44] Although a different recipe was used for each preparation, a typical synthesis involved the use of 100 mL of 3×10^{-4} M $Zn(AOT)_2$ solution in isooctane containing 0.9 mL of water (corresponding to W_O =10 where W_O = [water]/[surfactant]) to which a second reverse micellar solution of 0.1 M AOT in isooctane containing 0.9 mL of 0.1 M Na_2S (W_O = 10) was added with constant stirring. The ratio of S^{2-}/Zn^{2+} was always 0.9:1.The solution at this time was clear and nonscattering. This step was followed by the introduction of 5.8 mg of the two-photon dye, ASPI−SH, into the reverse micellar solution with vigorous stirring to ensure complete dissolution of the dye in the solution. The last step is the addition of tetraethyl orthosilicate (TEOS) where the molar ratio of TEOS:base is 1:1 and the molar ratio of TEOS:water is 1:20. The reaction was left for 12 h with stirring to ensure complete hydrolysis of TEOS. It is important to note that the TEOS reaction rate is much slower in the microemulsions as compared to that in the Stobers process.[45] The extraction of the nanocomposite particles was typically done by the addition of a water:ethanol (1:3) solution at pH 8, followed by extensive washing with the same solution to remove the surfactant and any unreacted dye. Finally, the composite nanoparticles were dispersed in a water solution of pH 8 for all measurements. At this pH, a negative charge is introduced on the surface of silica, which prevents aggregation by electrostatic repulsion.

Optical Spectra. The absorption spectra were recorded at room temperature using a Shimadzu UV−vis 300 spectrophotometer, with a resolution of ~1 nm. The spectra were obtained using a quartz cuvette (1-cm path length). Samples for optical spectra were prepared by dispersing the washed nanocomposite particles with water (pH = 8) and DMF. The emission spectra were collected on a SLM 48000MHF spectrofluorimeter using a xenon arc lamp as the excitation source. A fluorimetric quartz cuvette was used for solution measurements.

Lifetime Measurements. The fluorescence lifetime of the samples was measured using a high-speed streak camera system with a 2-ps time resolution (Model C 5680, Hamamatsu). The excitation light source was a series of laser pulses of ~398-nm wavelength and ~135-fs duration provided by a frequency-doubled mode-locked Ti:sapphire laser (Spectra Physics) system.

Confocal Microscopy. Image was obtained using a commercial confocal laser scanning microscope head (CLSM, Bio-Rad model MRC-1024), which was attached onto an upright microscope (Nikon, model Eclipse E800). A water immersion objective lens (Nikon, Fluor-60X Numerical Aperture = 1.0) was used for cell imaging. The system was adapted for two-photon excitation by using dichroic mirror sets from Bio-Rad. A broad band-pass filter (460−600 nm) was used as an emission filter. The excitation light was provided by a home-built mode-locked Ti−sapphire laser tuned to 800 nm, operating at 80-fs pulse width and 90-MHz repetition rate.

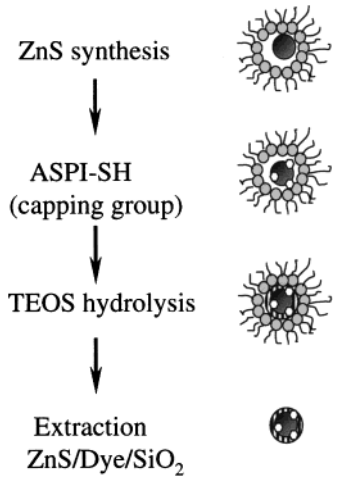

Figure 2. Schematic of the reverse micelles mediated synthesis of the two-photon encapsulated silica nanobubbles having a heterolayered structure.

Transmission Electron Microscopy. A JEOL JEM 2020 electron microscope operating at an accelerating bias voltage of 200 kV was used to collect transmission electron microscopic (TEM) images. Copper grids (200 mesh) coated with ~50-Å amorphous carbon film were purchased from Electron Microscopy Sciences. Samples were prepared by placing a drop of a dilute aqueous dispersion (pH = 8) of the composite nanoparticles on the surface of the grid placed on a piece of filter paper.

Result and Discussion

Figure 2 gives a schematic representation of the reverse micelles mediated synthesis of dye-doped composite nanoparticles. The TEM micrographs shown in Figure 3a indicate that the ZnS/dye/SiO_2 nanoparticles are fairly uniform in size and spherical in shape. The size of the particles is typically ~20 nm. The TEM picture also shows the core−shell structure present in these particles. The core is composed of ultrasmall zinc sulfide nanoparticles having a zinc blend structure that can be seen through electron diffraction of these particles. The size of the core is roughly 8 nm and is composed of zinc sulfide nanoparticles of size 2−3 nm, as determined by X-ray diffraction measurements. The thickness of the silica shell can be easily controlled by varying the molar ratio of water:TEOS. Preparation of nanosized composites from reverse micelles/microemulsion essentially involves various stages that differ in both nature and kinetics. While the core particles (ZnS) are formed by homogeneous nucleation and growth, the silica shell is formed by heterogeneous nucleation and growth.[46] The nucleation and growth of ZnS core particles involves a diffusion-controlled process through intermicellar interaction. Once the zinc sulfide particles of a desired size (W_0 =10) have been obtained, the two-photon dye (ASPI−SH) capping reagent, which binds

(44) Nelen, A. A. M.; Tavernier, S. M. F.; Gijbels, R. *Bull. Soc. Chim. Belg.* **1979**, *88*, 31.

(45) Stober, W.; Fink, A.; Bohn, E. *J. Colloid Interface Sci.* **1968**, *26*, 62−69.

(46) Li, T.; Moon, J.; Morrone, A. A.; Mecholsky, Talham, D. R.; Adair, J. H. *Langmuir* **1999**, *15*, 4328−4334.

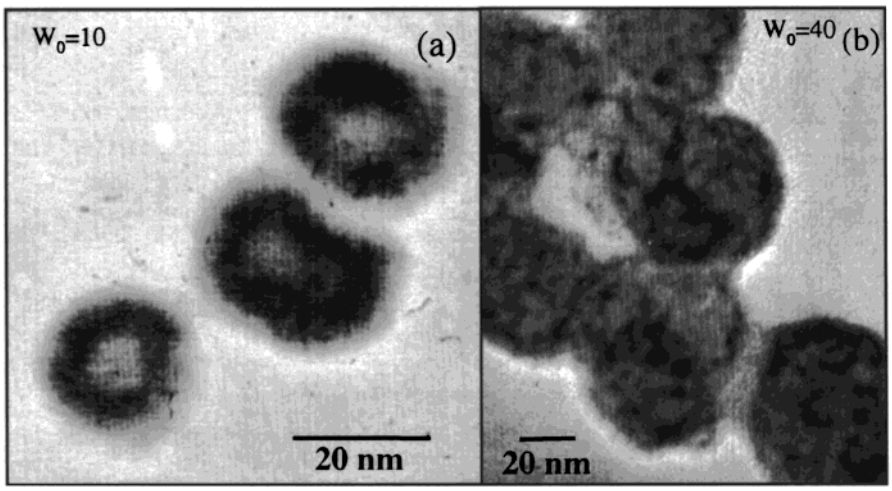

Figure 3. Transmission electron micrographs of two-photon dye-encapsulated silica nanobubbles synthesized at different droplet sizes: (a) $W_0 = 10$; (b) $W_0 = 40$. The nanoparticles at $W_0 = 10$ have a core−shell structure while the nanoparticles prepared at $W_0 = 40$ have a raspberry-type appearance.

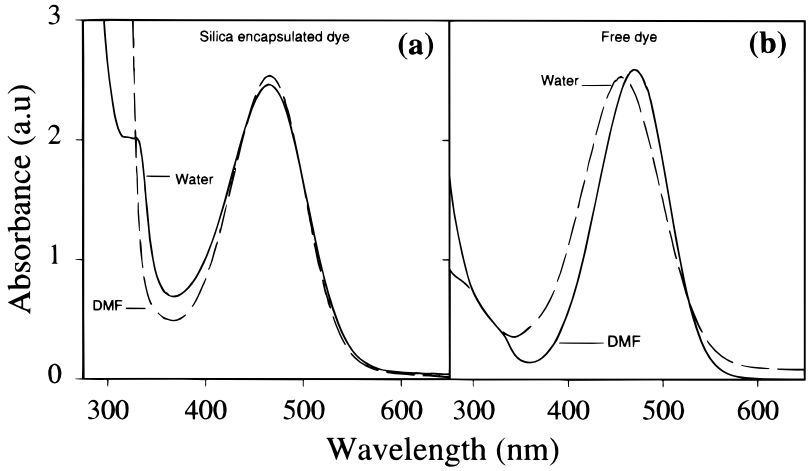

Figure 4. Comparison of the UV−vis absorption spectra of (a) a silica-encapsulated two-photon dye nanobubble and (b) the free two-photon dye in different solvents (water and dimethyl formamide) under identical conditions.

to the surface of nanocrystallites through the thiol group, is introduced. Capping groups present a significant steric barrier to the surface of a growing crystallite by slowing down the growth kinetics. Therefore, the dye (ASPI−SH) has a dual role: providing luminescence as well as controlling the growth of particles, resulting in highly uniform cores (∼8 nm) as seen in Figure 3a. For TEOS hydrolysis, it may be assumed that reverse micelles/micellar aggregates are not affected by the addition of TEOS. In other words, the shape of the reverse micelles remains unchanged.[47] Thus, under this assumption, the TEOS alkoxide molecules interact quickly with the water molecules inside the reverse micelles, forming a partially hydrolyzed silica shell around the dye-capped zinc sulfide nanoparticles. The thickness of this silica shell is dependent on the rate of condensation of the hydrolyzed species, which is a function of the molar ratio of water:TEOS governed by the water content of reverse micellar droplets. In fact, regulation of the water content of reverse micelles induces a structural change in the morphology of the nanocomposites as shall be seen later.

Figure 3b shows the TEM micrograph of a composite particle where the dye-capped zinc sulfide nanoparticles are homogeneously distributed over the silica surface, giving a raspberry type structural appearance. Here, the dye-doped nanosized composite particles were prepared at $W_0 = 40$ where the synthesis of the core zinc sulfide particles by coprecipitation within reverse micelles leads to the formation of several ZnS nuclei of size 8 nm. Also, because at this large droplet size ($W_0 = 40$) more free water is available for hydrolysis, the condensation reaction becomes predominantly an intramicellar process as opposed to an intermicellar one and competes with the aggregation mechanism of the zinc sulfide nuclei. The result is the formation of silica particles having homogeneous inclusions (instead of a core) of dye-capped zinc sulfide nanoparticles.

Figure 4 a,b shows the absorption spectra of the silica-encapsulated dye particles and the free dye in different solvents (DMF and water). As can be seen from the spectra, in the case of the free dye (Fig. 4b), the absorption maximum shows a blue shift with increasing solvent polarity, from DMF (dimethyl formamide) to water (from 470 to 455 nm, respectively). This behavior has been explained to be due to the fact that ASPI−SH is solvatochromic; i.e., it shows a solvent-dependent shift

(47) Adair, J. H.; Li, T.; Kido, K.; Havey, K.; Moon, J.; Mecholsky, J.; Morrone, A. *Mater. Sci. Eng.* **1998**, *23*, 139−242.

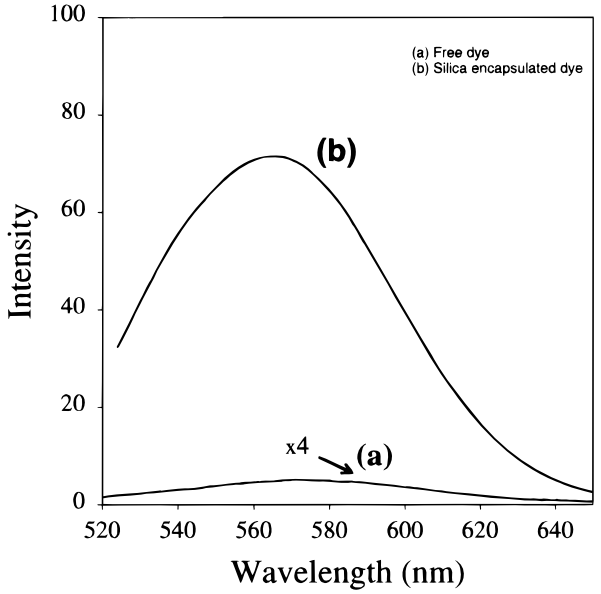

Figure 5. Fluorescence spectrum of (a) the silica-encapsulated dye (zns/dye/silica) and (b) the free dye (ASPI−SH) in water. The fluorescence spectra of the free dye has been increased by a factor of 4 (to bring into scale), indicating a marked decrease in the fluorescence yield in the case of the free dye in water compared to the that of the silica-encapsulated dye.

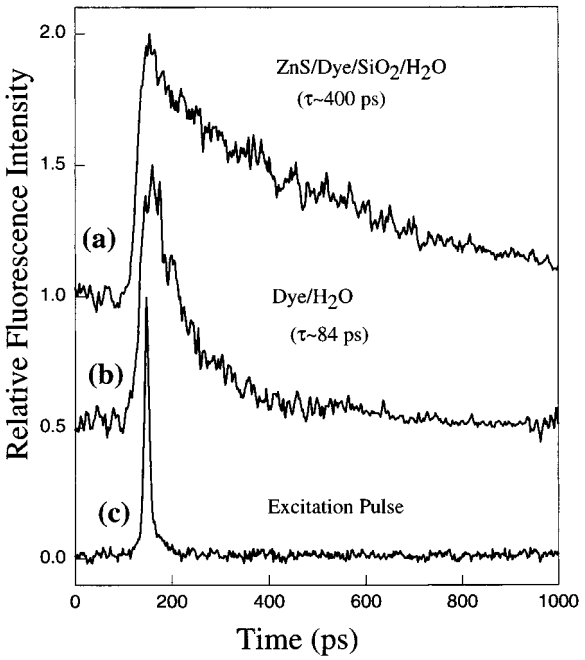

Figure 6. Fluorescence decay curves for (a) the silica-encapsulated dye and (b) the free dye in water using a frequency-doubled mode-locked Ti:sapphire laser.

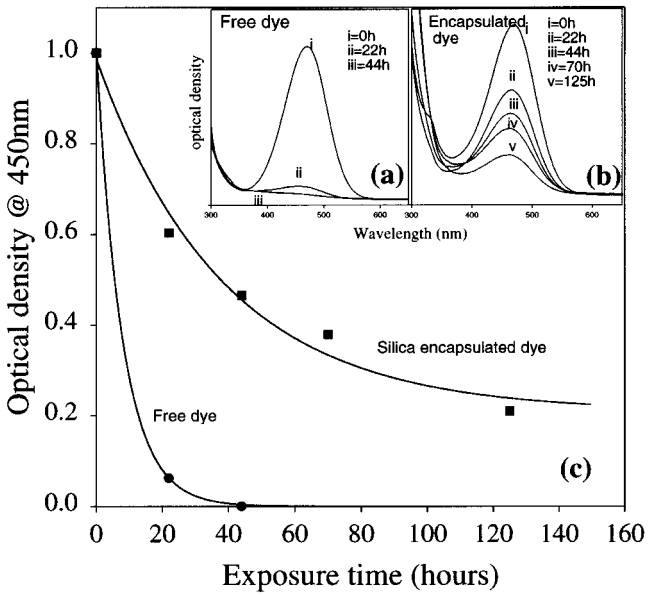

Figure 7. Photobleaching spectrum and comparison of the relative stabilities of (a) the free dye and (b) the silica-encapsulated dye and (c) the decay curve of the two samples as a function of time after exposing the samples to UV light (λ = 3500 Å).

in the absorption spectra, which is a characteristic feature of zwitterionic hemicyanine[34,35] type dyes. This phenomenon is attributed to a relatively high polar mesomeric form, which is predominant in the ground state. As a result, the hydrogen bond donating (HBD) solvents decrease the energy of the ground state, by acting as proton donors, leading to a blue shift[35] of the absorption band. The fluorescence spectrum of the pure dye (Figure 5a) also shows low quantum yield relative to the encapsulated dye. This behavior has been explained to be due to certain nonradiative decay mechanisms that may arise as a result of "twisted intramolecular charge geometry" acquired by the dye as a result of electron transfer from the donor group to the acceptor group. According to the "twisted intramolecular charge transfer" (TICT) model,[48] these molecules undergo an intramolecular transfer of an electron from the donor to the acceptor in the excited state, which is accompanied by a twist around the bond joining the donor and acceptor. In our case, the studied chromophore ASPI−SH contains an electron-donating amino group (one end) and electron-withdrawing group at the other end. The extent of the charge transfer process is strongly dependent on the polarity of the solvent; i.e., the activation barrier for the TICT process decreases with the increasing solvent polarity. As a result, with an increase in the polarity, the predominant TICT state, which is less emissive, produces a marked decrease in fluorescence yield. A similar effect has also been observed in the previous work from our group.[35]

In the case of dye-encapsulated silica nanoparticles, it is observed that there is a strong absorption around 320 nm corresponding to zinc sulfide nanoparticles and the spectral distribution of the dye-encapsulated silica nanoparticles in two solvents are the same (Figure 4b). In other words, there is no solvatochromic effect observed in the encapsulated particles, thereby supporting the assumption that the direct chemical environment of the dye molecule is independent of the external solvent environment. However, relative emission of these particles as seen in Figure 5b was always higher (70 times) than that of free dye solution. This behavior could possibly be due to the protective barrier provided by silica, as a result of which the dye is protected from the external solvent influence. Hence, the nonradiative decay processes, which are solvent dependent and are responsible for low fluorescence yield, are prevented.

(48) Song, Q.; Evans, C. E.; Bohn, P. W. *J. Phys. Chem.* **1993**, *97*, 13736.

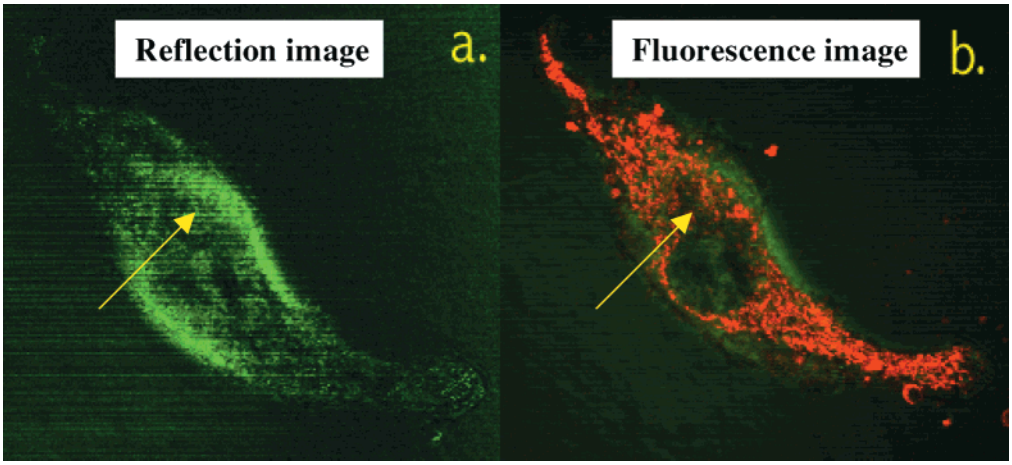

Figure 8. Reflection (green) and fluorescence (red) images of KB (human epithelial oral carcinoma cells) cells treated with silica nanobubble probes with the two-photon dye, ASPI−SH, using a two-photon laser scanning microscope (the yellow arrow indicates th eposition of the nucleus).

To get more insight into the radiative and nonradiative decay processes, we also conducted time-resolved lifetime experiments. Figure 6 shows the measured fluorescence decay curves for the free dye as well as the dye encapsulated within silica nanobubbles. The fluorescence decay as seen from Figure 6 is exponential and the lifetime was obtained by measuring the interval between the fluorescence intensity peak and the 1/e position. It was observed that the lifetime (300 ps) of the encapsulated dye particles was significantly longer than that that of the free dye molecule, indicating that the dye particles were shielded from the outside environment. This observation confirms that nonradiative decay processes responsible for quenching the emission are considerably reduced by silica encapsulation.

By silica encapsulation the chromophore also becomes more stable against chemical reaction. We performed a photobleaching experiment and compared the relative stabilities of the free dye and the silica-capsulated dye. It has been reported that photobleaching of a chromophore is often caused by a photooxidation[39] reaction. Therefore, if silica can effectively reduce the penetration of oxygen inside by forming a shell, the photobleaching process should be greatly reduced. We used pure dye solution and silica-encapsulated dye dispersion in DMF. Because DMF usually contains a large quantity of dissolved oxygen, no treatment for supplying oxygen into the solution was required. The two samples were put in a UV chamber ($\lambda = 3500$ Å) and changes in the absorption spectra were recorded as a function of exposure time. Figure 7c shows the change in the absorption spectrum as a function of time. Insets of Figure 7a,c indicate the change in the absorption peak for the free dye (a) and the silica-encapsulated dye (b) with time. As seen from the two figures, the absorption peak of the free dye totally disappeared within 50 h, but in the case of silica-capsulated dye, 20% of its initial value was retained, even after 120 h. These results indicate that the silica capsule increases the stability of the chromophore against the photobleaching reaction. This effect can be utilized for various applications involving dyes, which are susceptible to photodegradation. However, it is necessary to do more detailed experiments to fully establish the mechanism for enhanced photostability.

These novel inorganic−organic composite nanoparticles not only show promise for material science but also can lead to a new class of fluorescence probes in biological imaging. Nanoparticles have drawn considerable attention for their applications in cell labeling[3,4] and imaging. The closely related probe to such nanocomposites are the dye-doped polystyrene nanoparticles, which are commonly used for cell labeling. However, the hydrophilic nature of our composite nanoparticles and thus their compatibility with aqueous systems give them much more flexibility to be used in biological systems. Silica has been known for its biocompatibility and usage as a carrier in drug delivery[49,50] and in immunoassay. Because the surface of silica can be easily functionalized with different groups,[41,42] it can also be attached to a variety of biospecies. In addition, with the silica coating, we can encapsulate dyes with different emission ranges and characteristics in a uniform manner in one silica nanobubble. We have done some preliminary studies on the application of such nanoparticles in cell imaging. Figure 8 shows the image of KB cells, which are human epithelial oral carcinoma cells treated with our nanobubble probes containing two-photon dye ASPI−SH. The staining of the cells can be observed after 2 h by a two-photon laser scanning microscope ($\lambda_{ex} = 800$ nm) using a mode-locked Ti−sapphire laser. Figure 8a shows the reflection image of the KB cell in the cell medium at pH = 7.4 while Figure 8b indicates the overlap of the fluorescence image (red) on the reflection image (green). The two-photon fluorescence of the dye-encapsulated nanoparticles was visible 2 h after the nanoparticles were injected into the cell medium (10^{-6} M). The accumulation of the nanoparticles in the cytoplasm and membranes was easily identified (though the exact mechanism is not clear at this point, it is probably endocytosis) while the localization in the nucleus was not observed (the yellow arrow indicates the position the of nucleus). The viability of the cells to the nanoparticles was verified by its morphology and by tryptan blue staining, which indicated that the cells were alive even 3 h after the treatment. Further work involving

(49) Shimada, M.; Shoji, N.; Takashi, A. *Anticancer Res.* **1995**, *15*, 109−115.
(50) Peterson, P. K.; Peterson, C. M.; Pope, J. A. E. *Proc. Soc. Experimental Biol. Med.* **1998**, *218*, 365−369.

surface modification and attachment of the dye-encapsulated silica nanobubbles to biomolecules for biological applications is currently being carried out in our laboratory.

Conclusions

It has been demonstrated that whe a simple reverse micelles approach is used, two-photon dyes can be easily incorporated inside nanometer-sized silica nanobubbles with varying morphology and control over the distribution of the dye within the nanobubble. Also, we can easily modify the recipe to prepare composite nanoparticles of different sizes. Furthermore, it has been demonstrated that the encapsulation of hydrophobic dyes within silica not only improves their water dispersability but also leads to an increase in emission lifetime and emission efficiency. The photobleaching results indicate an increase in the photostability of the dye in the silica nanobubbles. The photostability can be further increased by increasing the thickness of the silica shell. The cell imaging results indicate that these silica nanobubbles can be effectively used as fluorescent probes for diagnostic applications.

Acknowledgment. This work was supported in part by the Air Force office of Scientific Research MURI program through the University of Southern California, primary contract 00057 and in part by the Directorate of Chemistry and Life Sciences of the Air Force office of Scientific Research through contract F496209610124.

CM000178K